JOURNAL OF THERMOPHYSICS AND HEAT TRANSFER
Vol. 24, No. 4, October–December 2010

New Inverse Model for Detecting Fire-Source Location and Intensity

Shaodong Guo,* Rui Yang,† and Hui Zhang‡
Institute of Applied Physics and Computational Mathematics, 100094 Beijing, People's Republic of China
and
Xin Zhang§
United Technologies Research Center, East Hartford, Connecticut 06108

DOI: 10.2514/1.46513

An inverse model and a procedure to detect fire location and determine fire intensity are developed. A time-dependent temperature database over the entire parameter space is generated using a fire simulation model. Then Markov chain Monte Carlo sampling based on Bayesian inferencing is used to determine parameters such as source location and strength. The probability distributions of source location and fire intensity are then calculated by inference using a Markov chain. Three test cases are used to evaluate the model. First, the model is validated using experimental data from the National Bureau of Standards multiroom test series for a simple setting involving a relatively small room and a long corridor. Second, a two-story office-building fire with 35 compartments is used to investigate the sensitivity and reliability of the model. Third, a high-rise building with a large space structure is used to improve the inverse model. It is shown that predicted fire source and intensity match the actual values for both constant- and varied-intensity fires. The effects of the sensors' sampling interval, intersensor spacing, measurement error, working range, and delay time on the sensitivity and reliability of the method are studied. The results indicate that a 50 s sampling interval generally results in high estimation performance with a relative error of 1%, but decreasing the intersensor spacing from 20 to 10 m does not significantly improve the accuracy of the inverse intensity if the sampling interval is small enough, such as 100 s. It is also found that using the sensor network with its lower upper limit less than 124°C leads to overestimation of the fire intensity. In addition, the accuracy of the predicted fire location is not affected by the accuracy of the forward fire model, while the accuracy of fire intensity predicted by the inverse model is sensitive to the systematic errors or the accuracy of the forward model.

Nomenclature

a	=	constant bias in systematic error of numerical model, K
b	=	scaling factor of varied component in systematic error of numerical model
C_p	=	constant-pressure specific heat, $m^2\ s^{-2}\ K^{-1}$
E	=	posterior expectation of source parameters, W
F	=	forward model prediction, K
$F_i^{(t)}$	=	numerical prediction for sensor i at time t, K
f	=	scalar function
$\bar{H}_L$	=	equivalent enthalpy in lower layer, J
$\bar{H}_U$	=	equivalent enthalpy in upper layer, J
$\dot{\bar{H}}_U$	=	change rate of equivalent enthalpy in upper layer, J/s
$\dot{\bar{H}}_L$	=	change rate of equivalent enthalpy in lower layer, J/s
h	=	height, m
h_{bot}	=	height of bottom of cold layer, m
h_{cold}	=	height of top of cold layer, m
h_{hot}	=	height of bottom of hot layer, m
h_{int}	=	height of the isoline for $f = 0.5$, m
h_{top}	=	height of top of hot layer, m
i	=	index of temperature sensor
k	=	number of temperature sensors
$\bar{M}_L$	=	equivalent mass in lower layer, kg
$\dot{\bar{M}}_L$	=	change rate of equivalent mass in lower layer, kg/s
$\bar{M}_U$	=	equivalent mass in upper layer, kg
$\dot{\bar{M}}_U$	=	change rate of equivalent mass in upper layer, kg/s
m	=	number of sampling points used to conduct inferences
N	=	number of iterations for Metropolis jump λ
n	=	number of instants in time
P	=	probability of source parameter
p	=	pressure, Pa
$P(\boldsymbol{T}\|\boldsymbol{X},\boldsymbol{F})$	=	the likelihood of the true temperature of sensor T, given the source parameter X and the modeled data F
$P(\boldsymbol{X})$	=	prior probability of source parameters
$P(\boldsymbol{X}\|\boldsymbol{Y})$	=	conditional probability of source parameters X given the measurement data Y
$P(\boldsymbol{Y})$	=	probability of the measurement data
$P(\boldsymbol{Y}\|\boldsymbol{X},\boldsymbol{T})$	=	the likelihood of the observed data Y, given the source parameter X and true temperature of sensor T
Q	=	fire intensity, W
q	=	proposed kernel
$q_{\alpha/2}$	=	lower bound of the highest posterior density interval
$q_{1-\alpha/2}$	=	upper bound of the highest posterior density interval
T	=	hot-gas-layer temperature, K
T_L	=	temperature in lower layer, K
$\bar{T}_L$	=	equivalent temperature in lower layer, K

Received 27 July 2009; revision received 4 June 2010; accepted for publication 9 June 2010.

*Ph.D. Candidate; guosd05@gmail.com.
†Associate Professor, Department of Engineering Physics, Center for Public Safety Research.
‡Professor, Department of Engineering Physics, Center for Public Safety Research.
§Senior Research Scientist.

T_{obs} = temperature measured by sensors, K
T_{sim} = temperature predicted by numerical model, K
$\bar{T}_U$ = equivalent temperature in upper layer, K
T_U = temperature in upper layer, K
$T_i^{(t)}$ = true value of sensor i at time t, K
t = time, s
t_0 = ignition reference time or fire beginning time, s
U = uniform probability distribution for random number generation
u = random number for Monte Carlo sampling
V = volume, m^3
V_L = volume of lower layer, m^3
V_U = volume of upper layer, m^3
var = posterior variance of the source parameters, W
$\boldsymbol{X}$ = vector of fire-source parameters, W
$\hat{\boldsymbol{X}}$ = estimator of source parameters with maximum probability, W
$\bar{\boldsymbol{X}}$ = mean value of source parameters, W
$\boldsymbol{X}^{(i)}$ = vector of fire-source parameters at ith time step, W
X_i = ith component of vector of source parameters, W
$X_i^{[(\alpha/2)n]}$ = estimator of lower limit of highest posterior density interval for ith component of vector of source parameters, W
$X_i^{[(1-\alpha/2)n]}$ = estimator of upper limit of highest posterior density interval for ith component of vector of source parameters, W
$\boldsymbol{Y}$ = vector of measurement data, K
$Y_i^{(t)}$ = observed data of sensor i at time t, K
$\boldsymbol{Z}$ = intermediate state sampled from proposal kernel, W
α = confidence probability within highest posterior density region
β = acceptance ratio
γ = specific heat ratio
δ = Dirac function
ε = fire growth rate, W/s^2
θ = acceptance probability
λ = standard deviation of Gaussian distribution for proposal kernel, Metropolis jump, W
$\lambda^{(i)}$ = standard deviation of Gaussian distribution for proposal kernel at ith time step, W
μ = mean of model and sensor error distribution, K
ξ = posterior joint probability of source parameters
$\bar{\rho}_L$ = equivalent density in lower layer, kg m^{-3}
$\bar{\rho}_U$ = equivalent density in upper layer, kg m^{-3}
σ = standard deviation of model and sensor error distribution, K
$\sigma_i^{(t)}$ = standard deviation of model and sensor error distribution for sensor i at time t, K
χ = whole space of source parameters

I. Introduction

ACCIDENTAL fires in buildings can lead to human fatalities and property loss unless prompt response measures are taken. However, proper response and strategy depend on the knowledge of fire location, fire intensity, and possible paths of the smoke. Furthermore, for some industrial buildings, such as warehouses with minimal human monitoring for extended periods, there is a critical need to automatically and quickly determine the presence of a fire. So an inverse fire-source model is needed that can offer a new approach to intelligent fire-detection systems, such as a video-based fire-detection system [1].

Inverse fire-detection methodology can be categorized into two approaches: direct and optimized approaches. The direct analytical approach solves heat transfer equations in reverse to obtain fire-source parameters. Davis et al. [2,3] developed a direct sensor-driven inverse fire model (SDFM) to predict the intensity of the fire based on signals from either smoke or heat sensors. The model gives the ceiling jet temperature as an analytical function of the location of the fire in the fire-source room and heat release rate. Then the analytical function is inverted such that the fire intensity is calculated from the measured temperatures or concentration of CO_2. In their model, the fire-source room needs to be known before inversion.

The other method, the optimized method, has been used to determine the fire-source parameters that are most probable through matching simulation and measurement. Richards et al. [1,4] developed an optimized method of solving the inverse fire-detection problem through minimizing the residuals between measured and predicted temperatures to give the most probable location and heat release rate of the fire. Because there are inevitable measurement errors and simulation errors, the uncertainty analysis is important. However optimization methods only give a single answer. Thus, these methods generally assume a Gaussian distribution to account for uncertainties or use perturbation methods [5,6], which is an obvious disadvantage of the optimization approach. Lee and Lee [7] developed a sequential inverse method to estimate the transient heat release rate and fire location. In their study, they used the sequential method combined with the concept of future time proposed by Yang [8] to improve the instability of the inverse method. The method in [7] is proved to be effective and efficient in the case of a single room building fire, although the accuracy of the determined fire intensity was sensitive to forward model errors and experimental errors.

In this paper, we present an alternate algorithm that uses a Markov chain Monte Carlo (MCMC) procedure that is based on a Bayesian probabilistic framework. This approach introduces the measurement error and the simulation error in a more straightforward manner than the optimization approach and gives the probabilities of the source parameters.

Compared with direct SDFM, there are two advantages of the MCMC method. First, the SDFM method is suitable for a single-room fire. However, for multiroom fires, the fire-source room needs to be given as prior information in the direct method. Then heat release rate and the height of the fire off the floor in the fire-source room can be estimated using an analytical function of ceiling jet temperature. However, when the sensor information is insufficient (for example, the fire-source room is unknown in multiroom building fire), in addition to the complicated nature of convective and radiative heat transfer typically found in multiroom fires, the direct analytical method may not be a good choice. In the MCMC method, the fire-source room, fire intensity, and fire height off the floor are all considered as random quantities, and they can be inverted simultaneously. The fire-source room can be assigned an unknown value before inversion. Thus, it is convenient to use the MCMC method for multiroom building fires. In contrast, the direct method cannot determine the fire-source room, fire intensity, and fire height simultaneously. Second, general fire inverse problems often include nonlinear processes. Traditional analytical methods have particular weaknesses in the cases of highly nonlinear systems or forward models and diverse data streams. The MCMC method imposes no restrictions on the types of models and data. Thus, highly nonlinear fire processes and disparate types of sensor data can be simultaneously incorporated into the analysis [5].

There are also two advantages of the MCMC method over the optimized method. First, uncertainty analysis of inversion method is important, considering the nature of the uncertainties or errors involved in both experimental and model sensor temperatures. For the optimization approach, uncertainty analysis requires many forward simulations and optimizations, resulting in a slow identification process. Unlike the optimized method, the MCMC method is a probabilistic method. In a Bayesian probabilistic framework, this approach introduces the measurement error and the simulation error in a more straightforward manner and yields a realistic estimate of the source parameters, including their uncertainty, more conveniently and efficiently. Second, both the optimization approach and the MCMC method relate the fire-source characteristics to the expected model temperatures at the sensors and the actual temperatures measured by sensors. The optimization approach accurately matches the model values to the actual measurements and gives a unique answer, while MCMC method establishes a relation between the

model values (subject to model errors) and the actual measured data (subject to measurement noise) using a probabilistic framework. Information about the source parameter probabilities encapsulated in the region surrounding the critical point can then be provided [9].

The MCMC technique is not new, and has been applied successfully to various fields. In the area of urban atmospheric diffusion, Chow et al. [5] first applied the inverse methodology based on Bayesian inference and Markov chain Monte Carlo sampling to determine the source for atmospheric release of hazardous materials in urban areas. However their method was very time-consuming. Keats et al. [9] introduced the adjoint equation to greatly increase the computational efficiency. They studied a steady-state concentration field to determine the release source. In practice, the concentration field is unsteady and the data from the sensors are time-varying in the early period of the release event; thus unsteady or dynamic inversion is necessary and essential for early warning and real-time identification of the source. Johannesson et al. [10] developed a dynamic Bayesian model via Monte Carlo, called the sequential Monte Carlo method, to determine the unsteady dispersion process of atmospheric release. But they used a rather simple Gaussian Puff model that resulted in an analytical solution for the adjoint equation. But this simple model could not characterize the complex flow field and special phenomena of concentration gradients coupled with the presence of buildings. Guo et al. [11] solved an unsteady adjoint transport equation by computational fluid dynamics (CFD) using adaptive mesh refinement combined with MCMC sampling algorithms. In the field of indoor air pollution source characterization, Liu and Zhai [12] developed a CFD-based adjoint probability method to identify instantaneous indoor contaminant point sources. Sohn et al. [13] was the first group to apply Bayesian inference to determine the location, intensity and duration of an indoor contaminant release in this field. In the field of health sciences and biostatistics, the chief difficulty in MCMC estimation is that any physiological model has a large number of parameters. To resolve this problem, Gelman et al. [14] proposed a new population physiological model and descriptive prior distributions. Their method increased the number of parameters but could take advantage of prior information on the parameters. In their physiological model, the distribution of parameters was a function of several population parameters, which reduced the number of parameters to be estimated. Their work provided an overview of issues involved in applying MCMC to biostatistics. In addition, in computer vision and image analysis, MCMC has played a prominent role as a means of calculation with image models [15].

However, the application of the MCMC approach to fire-source detection and smoke propagation prediction has not, to our knowledge, been reported in the literature. Of course, there are some pitfalls in Markov chain simulation: the stationary distribution of the Markov chain may not be the same as the desired target distribution of parameters; and the simulation may iterate many times in regions influenced by initial distributions [16]. Thus, the objective of this article is to validate the application of the MCMC model to fire detection using real experimental data and investigate the sensitivity and reliability of the model to different types and characteristics of sensor networks.

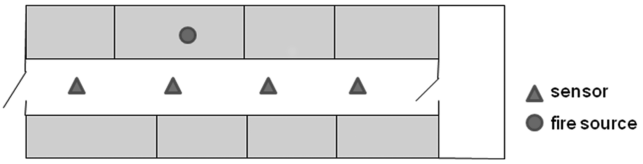

Fig. 1 Fire-source inverse illustration.

II. Fundamentals of the Inverse Model

The fire-source location and intensity reconstruction problem is illustrated in Fig. 1. When a fire occurs accidentally in a building, shown in Fig. 1, hot smoke rises due to the buoyant effect to form a hot layer near the ceiling. As time progresses, the hot smoke flows out of the door into the adjacent corridor and produces a thin jet along the ceiling in the corridor. The temperature sensors located at the ceiling can provide different measurement data due to their different distances to the fire source. The objective of the inverse model is to locate the fire-source and identify the fire release rate according to the multiple readings of the sensors with different locations and times. Unlike direct sensor-driven inverse fire models (SDFM), in our method, fire location and heat release rate (HRR) are both considered as random quantities and estimated simultaneously (not in sequence). The probabilities of fire location and HRR are computed simultaneously according to how well model predictions agree with multiple readings from the sensors.

A. General Framework

In the introduction to the inverse model, a flowchart is given in Fig. 2 to show how Sec. II provides the general framework of the inverse model. As can be seen, the inverse model is divided into two steps: forward simulation and backward inference. First, in the forward simulation step, a proper forward model is selected to calculate instances of predicted sensor measurement $\boldsymbol{Y}$ at the sensors for given possible fire-source parameters $\boldsymbol{X}$. In this step, many fire scenarios are simulated, and temperatures $\boldsymbol{Y}$ due to different fire inputs $\boldsymbol{X}$ are stored in a database. Any uncertain fire forward model input parameters, such as the fire size, the fire location, the fire growth rate, the size of the door opening and window openings, etc., need to be assigned uncertainty distributions. Then the fire database can be generated using different fire input parameters sampled from the assigned distributions. In our model, heating, ventilation, and air conditioning effects are not considered. This step can be implemented before inversion calculation although the number of the parameters is large, which will cause a large number of forward simulations to be performed. Of course, when the parameter number

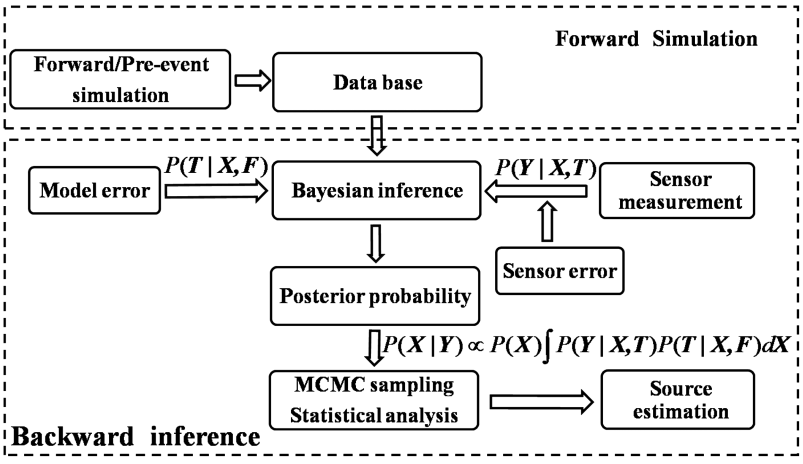

Fig. 2 Flowchart of the inverse model.

increases, the database becomes large. More time is needed to create the database.

The second step is the backward inference process. Our methodology for this step is based on Bayesian inference combined with a Markov chain Monte Carlo sampling procedure. When a fire occurs, the temperature or concentration can be provided by sensors distributed in buildings. With both the sensor measurement data and modeled data of each possible fire-source parameter, which can be obtained from the stored database in the first step, the posterior probabilities of source parameters can be estimated using Bayesian inference. The efficiency of the model mainly depends on the second step, backward inference, since the first step, forward simulation, can be completed beforehand. During the second step, the temperature or concentration from possible fire-source parameters can be obtained directly from the database generated in the first step. Thus, the inversion step is quick and can be performed in real time.

B. Bayesian Inference and Posterior Probability

The Bayesian theorem is used to determine the probability of an event $\boldsymbol{X}$ occurring conditioned on another event $\boldsymbol{Y}$ [5]:

$$P(\boldsymbol{X}|\boldsymbol{Y}) = \frac{P(\boldsymbol{Y}|\boldsymbol{X})P(\boldsymbol{X})}{P(\boldsymbol{Y})} \propto P(\boldsymbol{Y}|\boldsymbol{X})P(\boldsymbol{X}) \tag{1}$$

Let $\boldsymbol{X} = \{X_1, X_2, \ldots, X_i, \ldots, X_n\}$ denote the fire-source parameters (location, intensity, fire start time, fire growth rate, and so on), and let $\boldsymbol{Y} = \{Y_1, Y_2, \ldots, Y_i, \ldots, Y_k\}$ denote the measurement data (temperature) from sensors. Then $P(\boldsymbol{X}|\boldsymbol{Y})$ characterizes the conditional probability distributions of fire-source parameters given the measurement data. $P(\boldsymbol{X})$ denotes the prior distribution of the source parameters, which is determined through all available prior information. $P(\boldsymbol{Y}|\boldsymbol{X})$ denotes the likelihood of observing the measurements $\boldsymbol{Y}$ given the fire-source parameters $\boldsymbol{X}$.

Let $Y_i^{(t)}$ denotes the observed data of sensor i at time t. $F_i^{(t)}$ denotes the forward numerical model prediction at sensor i at time t. Both measurements and simulations have errors that are assumed to have independent Gaussian distributions with zero mean and standard deviations $\sigma^{(t)}$ at time t. Let $T_i^{(t)}$ denote the true value at sensor i at time t. The likelihood function can be derived as follows [9]:

$$P(\boldsymbol{Y}|\boldsymbol{X}) = P(\boldsymbol{Y}|\boldsymbol{X}, \boldsymbol{T})P(\boldsymbol{T}|\boldsymbol{X}, \mathbf{F}) = \prod_{t=1}^{n}\prod_{i=1}^{k} P(Y_i^{(t)}|\boldsymbol{X})$$

$$\propto \exp\left\{-\sum_{t=1}^{n}\sum_{i=1}^{k}\frac{[F_i^{(t)}(\boldsymbol{X}) - Y_i^{(t)}]^2}{2\sigma_i^{(t)2}}\right\} \tag{2}$$

Substituting Eq. (2) for Eq. (1), the posterior distribution of fire-source parameters can be obtained as follows:

$$P(\boldsymbol{X}|\boldsymbol{Y}) = P(\boldsymbol{X})\exp\left\{-\sum_{t=1}^{n}\sum_{i=1}^{k}\frac{[F_i^{(t)}(\boldsymbol{X}) - Y_i^{(t)}]^2}{\sigma_i^{(t)2}}\right\}/P(\boldsymbol{Y}) \tag{3}$$

where

$$P(\boldsymbol{Y}) = \int P(\boldsymbol{Y}|\boldsymbol{X})P(\boldsymbol{X})\,\mathrm{d}\boldsymbol{X}$$

$$\propto \int \exp\left\{-\sum_{t=1}^{n}\sum_{i=1}^{k}\frac{[F_i^{(t)}(\boldsymbol{X}) - Y_i^{(t)}]^2}{2\sigma_i^{(t)2}}\right\}P(\boldsymbol{X})\,\mathrm{d}\boldsymbol{X} \tag{4}$$

C. MCMC Sampling

At this point, the final form of the posterior probabilities of the source has been obtained. The Markov chain technique is used to generate a collection of realizations that has the posterior distribution of the source path as its limiting stationary distribution. The samples in the chain can then be used to conduct inferences. In this paper, we implement the MCMC scheme using the Metropolis–Hastings sampling algorithm, which is applied to generate a Markov chain. Practical implementation of the Metropolis–Hastings algorithm [5] is as follows:

1) If $i = 1$, fix $\boldsymbol{X}^{(0)}$.

2) Construct proposed kernel $q(\boldsymbol{X}^{(i-1)})$ where $q(\boldsymbol{X}^{(i-1)})$ is a Gaussian distribution function $\boldsymbol{X}^{(i)} \sim \text{Gaussian}(\boldsymbol{X}^{(i-1)}, \lambda^{(i-1)^2})$, and λ is adaptively updated every N iterations according to the current acceptance ratio β as follows:

$$\lambda^{(i+N)} = \begin{cases} 0.1\lambda^{(i)} & 0 \le \beta < 0.001 \\ 0.5\lambda^{(i)} & 0.001 \le \beta < 0.05 \\ 0.9\lambda^{(i)} & 0.05 \le \beta < 0.2 \\ \lambda^{(i)} & 0.2 \le \beta < 0.5 \\ 1.1\lambda^{(i)} & 0.5 \le \beta < 0.75 \\ 2.0\lambda^{(i)} & 0.75 \le \beta < 0.95 \\ 5.0\lambda^{(i)} & 0.95 \le \beta \le 1.0 \end{cases}$$

where

$$\beta = \frac{\text{no. of acceptances}}{\text{no. of iterations}}$$

3) Simulate state $\boldsymbol{Z}$ from density $\boldsymbol{Z} \sim q(\boldsymbol{X}^{(i-1)})$.

4) Calculate acceptance probability $\theta(\boldsymbol{X}^{(i-1)}, \boldsymbol{Z})$ from

$$\theta(\boldsymbol{X}, \boldsymbol{Z}) = \min\left[1, \frac{\xi(\boldsymbol{Z})q(\boldsymbol{Z}, \boldsymbol{X})}{\xi(\boldsymbol{X})q(\boldsymbol{X}, \boldsymbol{Z})}\right]$$

where $\xi(\boldsymbol{X}) = P(\boldsymbol{X})P(\boldsymbol{Y}|\boldsymbol{X})$.

5.) Decide acceptance. For this, generate $u \sim U(0, 1)$. If $u \le \theta(\boldsymbol{X}^{(i-1)}, \boldsymbol{Z})$, then accept transition: $\boldsymbol{X}^{(i)} = \boldsymbol{Z}$; else $u > \theta(\boldsymbol{X}^{(i-1)}, \boldsymbol{Z})$, then stay in the present state $\boldsymbol{X}^{(i)} = \boldsymbol{X}^{(i-1)}$.

6) If $i = i + 1$, go to step 2.

After a sample $\boldsymbol{X} = \{\boldsymbol{X}^{(1)}, \boldsymbol{X}^{(2)}, \cdots, \boldsymbol{X}^{(i)}, \cdots, \boldsymbol{X}^{(m)}\}$ from the posterior distribution of the source term is obtained, it can be used to conduct inferences and make statistical analysis The posterior joint distribution is

$$\xi(\boldsymbol{X}) = \frac{1}{m}\sum_{i=1}^{m}\delta(\boldsymbol{X}^{(i)} - \boldsymbol{X}) \tag{5}$$

The posterior expectation of the source parameters is

$$E(\boldsymbol{X}|\boldsymbol{Y}) = \int_{\chi} \boldsymbol{X}P(\mathrm{d}\boldsymbol{X}|\boldsymbol{Y}) = \int_{\chi} \boldsymbol{X}\,\mathrm{d}\xi = \frac{1}{m}\sum_{i=1}^{m}\boldsymbol{X}^{(i)} \tag{6}$$

The estimator of source parameters with maximum probability is

$$\hat{\boldsymbol{X}} = \arg\max \xi(\boldsymbol{X}) \tag{7}$$

The posterior variance of the source parameters is

$$\text{var}\,(\boldsymbol{X}|\mathbf{Y}) = \int_{\chi}(\boldsymbol{X} - E(\boldsymbol{X}|\mathbf{Y}))^2\,\mathrm{d}\xi = \frac{1}{m}\sum_{i=1}^{m}(\boldsymbol{X}^{(i)} - \bar{\boldsymbol{X}})^2 \tag{8}$$

The highest posterior density (HPD) interval provides a natural analogy to classic confidence interval within the Bayesian framework. The HPD region of content $P = 1 - \alpha$ is defined as $P(q_{\alpha/2} < X_i \le q_{1-\alpha/2}) = 1 - \alpha$. Then the elements of the ordered Markov chain, $[X_i^{[(\alpha/2)m]}, X_i^{[(1-\alpha/2)m]}]$, can define the estimated confidence interval.

D. Forward Model and Pre-Event Simulation

The inversion procedure relies on a forward model to calculate instances of predicted sensor measurement $\boldsymbol{Y}$ at sensors for given fire-source parameters $\boldsymbol{X}$. The fire-zone models CFAST (consolidated model of fire and smoke transport) [17] and the three-layer model [18] are used to simulate smoke propagation and predict temperature and concentration in building fires. Zone models have been used to simulate fires in multistory buildings, single rooms, and multirooms. The governing equations of the three-layer model are derived using the conservation of mass and energy, the ideal-gas law, and the relations for density and internal energy:

$$\frac{\mathrm{d}p}{\mathrm{d}t} = \frac{\gamma - 1}{V}(\dot{\bar{H}}_L + \dot{\bar{H}}_U) \tag{9}$$

$$\frac{\mathrm{d}V_U}{\mathrm{d}t} = \frac{1}{\gamma p}\left[(\gamma - 1)\dot{\bar{H}}_U - V_U\frac{\mathrm{d}p}{\mathrm{d}t}\right] \tag{10}$$

$$\frac{\mathrm{d}T_U}{\mathrm{d}t} = \frac{1}{C_p\bar{\rho}_U V_U}\left(\dot{\bar{H}}_U - C_p\bar{T}_U\dot{\bar{M}}_U + V_U\frac{\mathrm{d}p}{\mathrm{d}t}\right) \tag{11}$$

$$\frac{\mathrm{d}T_L}{\mathrm{d}t} = \frac{1}{C_p\bar{\rho}_L V_L}\left(\dot{\bar{H}}_L - C_p\bar{T}_L\dot{\bar{M}}_L + V_L\frac{\mathrm{d}p}{\mathrm{d}t}\right) \tag{12}$$

Equations (9–12) are similar to those of the two-layer model in CFAST. But all of the terms on the right-hand sides of the equations use integrally averaged properties such as $\bar{T}_U, \bar{T}_L, \bar{H}_L, \bar{H}_U, \bar{M}_U, \bar{M}_L$, which are different from those of the two-layer model. They are computed as follows:

$$\bar{T}_L = \frac{h_{\mathrm{cold}} - h_{\mathrm{bot}}}{h_{\mathrm{int}} - h_{\mathrm{bot}}}T_L + \frac{1}{h_{\mathrm{int}} - h_{\mathrm{bot}}}\int_{h_{\mathrm{cold}}}^{h_{\mathrm{int}}}[T_U f + T_L(1-f)]\,\mathrm{d}h \tag{13}$$

$$\bar{T}_U = \frac{h_{\mathrm{top}} - h_{\mathrm{hot}}}{h_{\mathrm{top}} - h_{\mathrm{int}}}T_U + \frac{1}{h_{\mathrm{top}} - h_{\mathrm{int}}}\int_{h_{\mathrm{int}}}^{h_{\mathrm{hot}}}[T_U f + T_L(1-f)]\,\mathrm{d}h \tag{14}$$

The formulas are similar for $\bar{H}_L, \bar{H}_U, \bar{M}_U$, and $\bar{M}_L$. In the three-layer model, f is a scalar function that is used to describe the smoke vertical profile so that physical properties such as temperature, smoke concentration and flow velocity can be represented and calculated. In general, the equation for f can be established and solved using volume of fluid or level-set method to obtain the distribution of f. The details can be found in [18].

III. Results and Discussion

In this section, experimental data and simulation-generated data will be used to evaluate and validate the inverse model.

A. Validation with Experimental Data from Multiroom Fire

The National Bureau of Standards (now National Institute of Standards and Technology) conducted a set of multiroom fire experiments [19,20]. The suite consisted of a relatively small room and a relatively long corridor. There was a 2.0 m high and 1.1 m wide door between the fire-source room and the corridor, and a 2.0 m high and 0.8 m wide door connecting the corridor to the outside. The multiroom configuration for this study is shown in Fig. 3. The dimensions of the compartments are listed in Table 1. The fire source, a gas burner, is located against the rear wall of the small compartment. For validation, experimental data for a 100 kW fire are selected because these tests had the steadiest values of measured heat release rate during the steady-burn period. The measurements are the hot-gas-layer (HGL) temperatures, and bare bead thermocouples were used for these measurements. Here, we assume that measurement errors are normally distributed (Gaussian distribution) with zero mean and a standard deviation $\sigma = 10$ K. In Fig. 3b, A and B denote the location of the sensors, including vertical arrays of eight thermocouples at each location that are used to produce the average HGL temperature using the HGL reduction method [20].

The zone model CFAST is used to perform forward simulation. In the model, the corridor is divided into five virtual rooms/zones, shown in Fig. 3. Each room is connected to its adjacent room through a fully open door. Figure 4 shows the comparison of the temporal variation of HGL temperature predicted by the forward model and experimental data. The figure indicates that the forward model has a systematic error in addition to the random error, especially for the location near the fire source (sensor A). It seems that the sensor should read a higher temperature than that computed by CFAST

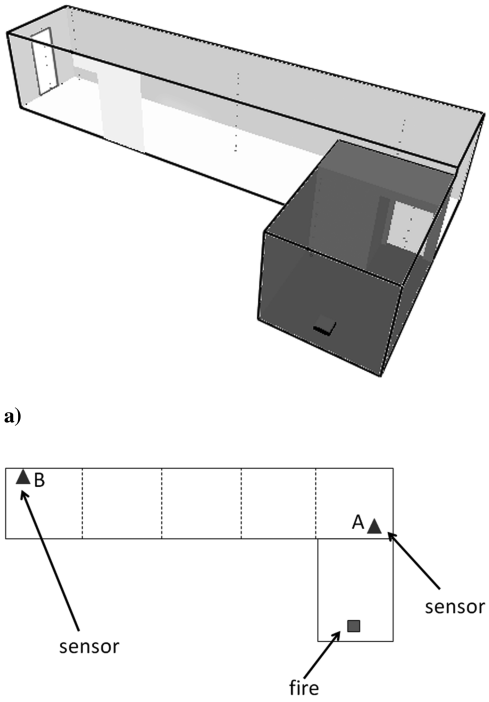

Fig. 3 Configuration of the multiroom case: a) 3-D view and b) plan view.

when the sensor location is closer to the fire than the center of the virtual room. However, there is a reason for the overprediction by CFAST. This is mainly attributed to the limitations of the two-layer assumption of CFAST, which uses two layers to describe a compartment: hot-smoke layer and cold-air layer. The model assumes that the predicted conditions in each layer have uniform properties and the momentum transport within and between the two layers are ignored. It is evident that as time progresses, the smoke and the cold air will mix rapidly within a small distance so that distinct layers will not be discernible. The two-layer model in CFAST is unable to accurately capture the mixture between the upper and the lower layers, which results in overprediction in the upper layer and underprediction in the lower layer [17], especially in a multiroom building with long corridors where smoke diffusion is significant. Thus, the two-layer assumption should be the main error source resulting in overestimation by CFAST.

To validate the inversion algorithms and to investigate the effect of systematic error on the accuracy of the inversion algorithms in predicting the fire location and intensity, both the modeling data with systematic error and experimental data are used.

Figure 5 shows the probability distribution (histogram) of the fire location predicted by the inverse model. From the figure, the fire location can be accurately identified as the actual fire room. Thus, systematic errors in the fire model have little effect on fire location errors. The reason is that in the fire location inverse algorithm, the relative HGL temperature of all sensors is more important than absolute HGL temperature. The forward model, whether or not there is a systematic error, will always predict the highest temperature at the sensor closest to the fire source, the second highest at the sensor next closest to the fire source, and so on. Therefore the accuracy of the fire location in the inverse model is not sensitive to systematic errors in the fire model.

Table 1 Dimensions of the building in test 1

Compartments	Width, m	Depth, m	Height, m
Fire room	2.4	3.4	2.2
Corridor	2.4	12.0	2.4

However, as shown in Fig. 6, different from the fire location, the accuracy of fire intensity predicted by the inverse model is significantly affected by the systematic errors or the accuracy of the forward model. From Figs. 4 and 6, we can see that if the fire forward model overestimates the HGL temperature, the inverse model will underestimate the fire intensity accordingly, which is also indicated in Table 2.

Since we used the Markov chain technique to generate a collection of samples of the source terms, these samples can then be used to conduct inferences and perform statistical analysis. The summary statistics are shown in Table 2. Within the Bayesian framework, the statistical quantities in Table 2 can be calculated using Eqs. (5–8). In this table, the 95% HPD interval denotes the shortest interval with the highest posterior probabilities in parameter space that contains 95% of the sampled values in the Markov chain. The 95% HPD interval is similar to the 95% confidence interval within the Bayesian framework, which means the posterior probability that the unknown parameter lies in the interval is 95%. The two numbers for the HPD interval denote the lower bound and upper bound.

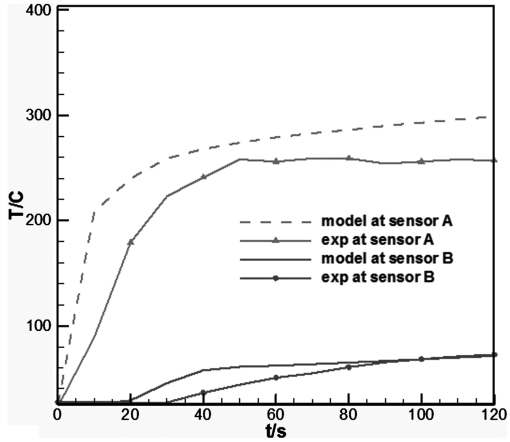

Fig. 4 HGL temperatures at sensors A and B predicted by the forward model and given by experimental data.

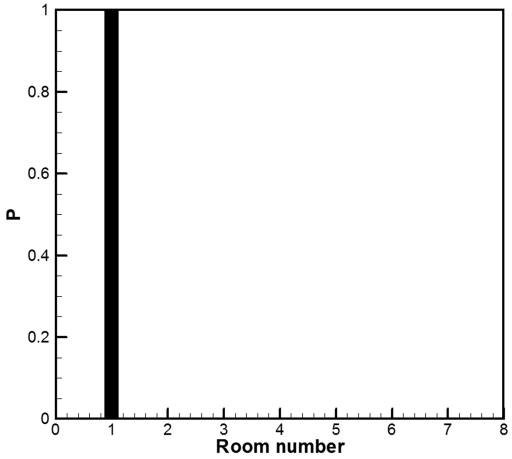

Fig. 5 Histogram (probability) of the fire location.

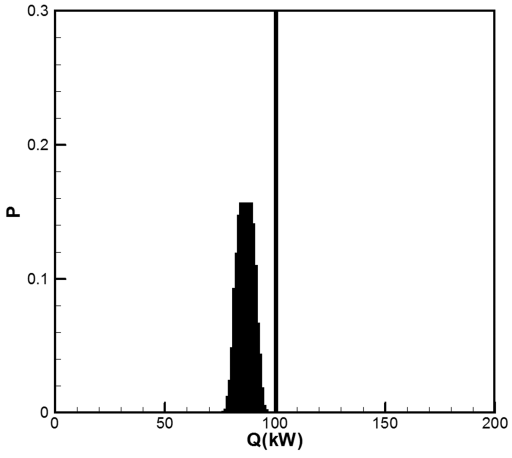

Fig. 6 Histogram (probability) of the fire intensity.

Table 2 The summary statistics of the determined fire intensity

	$E(\mathbf{X}\|\mathbf{Y})$, kW	$\hat{\mathbf{X}}$, kW	var$(\mathbf{X}\|\mathbf{Y})$, kW	95% HPD interval, kW
Model	86.799	87.00	2.502	[81.729, 91.484]
True	100	——	——	——

Here, we have demonstrated successful inversion of fire-source location using experimental data. Although the accuracy of the fire intensity predicted is affected by the inaccuracy of the fire forward model, the backward inference of the inverse model itself is reliable; and if the accuracy of the forward model is increased or the systematical error of the forward model is considered, the determined fire intensity will be improved accordingly.

CPU time required by the inverse model is an important factor. Since the computationally intensive forward simulations can be completed before a fire occurs, the efficiency of the inverse approach mainly depends on the backward inference and the MCMC sampling procedure during a fire event. Generally, when the number of source parameters is not too large, the inverse procedure can be completed within several seconds using ordinary PC. For example in this case, the whole data interpretation process only takes 9 seconds. Thus, the inversion can be efficient and become almost real time when the sensor data streams into the inverse model during the fire.

B. Test 2: Sensibility and Reliability of the Inverse Model for Complex Building

In this section, a more complex building with more compartments is used to assess the sensibility and reliability of the inverse model. Figure 7 illustrates the lower floor map of an office building in the United Technologies Research Center (E. Hartford, CT, U.S.A.). There are 35 compartments and 3 corridors, two of which are connected to a lobby at the left side of the building. Corridor 26 has a height of 2.67 m, a width of 2.4 m, and a length of 59.7 m. Corridor 27 has a height of 2.67 m, a width of 2.0 m, and a length of 19.4 m. Corridor 28 has a height of 2.67 m, a width of 2.4 m, and a length of 49.0 m. All sensors are assumed to be flush with the ceiling and provide temperatures as time progresses. Measurement errors with a normal distribution are also added (in this case with mean $\mu = 0$ and standard deviation $\sigma = 0.5$ K).

The fire source was located in room 10. Because the geometry of the building provided by United Technologies Research Center was that 25 rooms were open and 10 rooms were closed, we used this geometry as prior information and assumed that fire only occurred in one of the 25 shaded compartments in Fig. 7. Prior probability of the fire-source room X was assigned as follows:

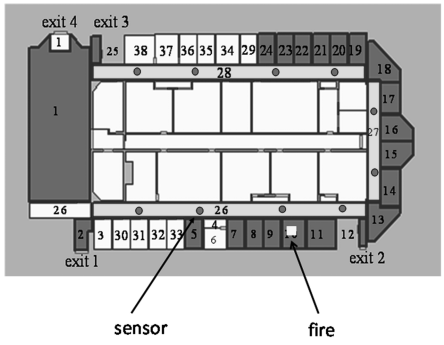

Fig. 7 Diagram of the building in test 2.

$$P(X) = \begin{cases} \frac{1}{25} & 1 \le X \le 25 \\ 0 & X > 25 \end{cases} \quad (15)$$

Although in this case only 25 rooms were chosen to be open, the model here is general and suitable for any number of rooms in this building. We also assumed that the heat release rate was less than 1 MW. A temperature library or database was generated through running 25×20 forward simulations using the three-layer model. Each simulation represented a possible fire configuration or scenario. This temperature database consisted of 25 possible fire locations, since 25 rooms in this building and 20 possible fire strengths from 0.05 to 1 MW were selected. Other possible fire strengths could be interpolated from this database. Next, we investigate the influence of different types and characteristics of the sensor network on the inverse model.

1. *Intersensor Spacing and Time-Sampling Interval*

We apply a uniform array of sensors installed on the ceiling of the three corridors. Nine cases are studied. In cases 1, 2, and 3, we fix the time-sampling interval to 50 s, and vary the intersensor spacing among 20, 10, and 5 m. In cases 4–6 and 7–9, we change the sampling time to 100 and 150 s, respectively, and also vary the intersensor spacing among 20, 10, and 5 m. The fire intensity is set to be a constant value of 0.4 MW.

Table 3 illustrates the statistics of the estimated fire intensity in nine cases. The definitions of the statistics are the same as those in Table 2. As expected, a small time-sampling interval results in high estimation performance. For example, as the interval reduces from 150 s in case 9 to 50 s in case 3, the mean fire intensity improves from 0.598 to 0.400 MW, and the standard deviation reflecting the uncertainty reduces from 0.22 to 0.014 MW. However, the sensors always have a minimum time interval at which they can measure the temperatures. Thus, the sensor time-sampling interval cannot be too low.

Another factor, intersensor spacing, also has impact on performance of the inverse model. It is shown that with the intersensor spacing decreasing, such as from case 7 to 8 and to 9, the mean intensity will get closer to the actual value, which is also expected. Another observation is that for the sensor network with smaller time-sampling intervals, such as cases 5 and 6, decreasing the intersensor spacing cannot improve the accuracy of the inverse intensity significantly enough to justify the increased cost of installing more sensors. That means there exists a financially optimal combination of time-sampling interval and intersensor spacing.

2. *Sensor Error and Sensitivity*

In this section, three cases are studied to explore the role of sensor error and sensitivity (detection limit). In cases 1 and 2, we assume there is no detection limit in the sensors, and the probability distributions of the sensor errors do not change. The error has a Gaussian distribution with zero mean and standard deviation σ. In case 1, $\sigma = 1.0$ K, denoting a higher uncertainty in the random error; in case 2, $\sigma = 0.5$ K, denoting a lower uncertainty. The time-sampling interval is 50 s, and the intersensor spacing is 10 m. The fire intensity is also set to a constant value of 0.4 MW.

From Figs. 8a and 8b, the advantage of the low-uncertainty sensor network is obvious. In case 1, the probability distribution based on data from the sensors with high uncertainty clearly illustrates that the sensor network predicts two clusters of possible fire intensity: one includes the correct source intensity, and the other includes a peak at the wrong source intensity. Furthermore, the distribution (histogram) is very flat, filling a broader range of the release rates considered. In case 2, the standard deviation σ is reduced from 1.0 to 0.5. The sensor data with low uncertainty narrows the field of probability within 0.3 to 0.5 MW. The peak probability is at the correct source intensity. Thus, in this case, the sensor network with low uncertainty can clearly identify the correct source intensity, while the sensor network with high uncertainty may provide insufficient information for distinguishing between two possible clusters of the source intensity.

Next, we fix the distribution of the sensor error ($\sigma = 0.5$ K), and investigate the effect of detection limit of the sensor network. In case 3, the sensor has an upper limit, or saturation level, which is set to 124°C. Case 2, where the sensor does not have a detection limit, is included for comparison.

From Figs. 8b and 8c, in case 3, the proposed method estimates a higher fire intensity level than the actual value and that of case 2. The reason is that all of the temperatures higher than the sensor limit are truncated to 124°C, as if part of the sensor network underestimates the temperature. Similar to the systematic errors of the fire model in Fig. 4 and 6, the inverse model overestimates the fire intensity accordingly. Therefore the sensor network with a lower upper limit decreases the estimation accuracy and has a significant impact on inversion results. A possible remedy is to detect the faulty sensor, eliminate the data from that sensor and then compensate the data loss using more readings in time.

3. *Variable Fire Intensity and Sensor Time Delay*

In previous sections, the fire-source intensity is constant. In a real fire, the intensity is generally time-varying. In particular, the growth phase of many fires can be characterized by a heat release rate increasing proportionally with the square of time measured from the ignition reference time t_0, as follows:

$$Q = \varepsilon(t - t_0)^2 \quad (16)$$

This relation has been validated in an extensive series of tests [21]. Thus, in this section, the square relation is used to describe the variable fire intensity. Here, we assume that the ignition reference time t_0 is known as prior information, which may be obtained through other sensing devices such as video cameras.

In practice, a time delay often exists due to propagation delay of the sensor network. In this section, the effects of the time delay of the sensor network on the accuracy of the inverse model will be investigated.

In cases 1 and 2, sensor time delay is not considered. In these two cases, we explore the reliability of the inverse model applied to variable fire intensity. The sampling interval is 20 s in both cases. In case 1, the intersensor spacing is 20 m. In case 2, the intersensor spacing is 10 m. In cases 3 and 4, we fix the intersensor spacing at 10 m, and vary the time delay of the sensor network between 10 and 20 s. Using these cases, along with case 2, in which the delay is 0 s,

Table 3 The summary statistics of the determined fire intensity in nine cases

	Intersensor space, m	Time-sampling interval, s	$E(\mathbf{X}\|\mathbf{Y})$, MW	var$(\mathbf{X}\|\mathbf{Y})$, MW	95% HPD interval, MW
Case 1	20	50	0.404	0.027	(0.353,0.460)
Case 2	10	50	0.400	0.019	(0.363,0.438)
Case 3	5	50	0.400	0.014	(0.373,0.424)
Case 4	20	100	0.630	0.211	(0.333,0.941)
Case 5	10	100	0.404	0.031	(0.346,0.466)
Case 6	5	100	0.403	0.021	(0.365,0.448)
Case 7	20	150	0.674	0.238	(0.336,0.999)
Case 8	10	150	0.613	0.247	(0.345,0.997)
Case 9	5	150	0.598	0.22	(0.279,0.999)
True	——	——	0.400	——	——

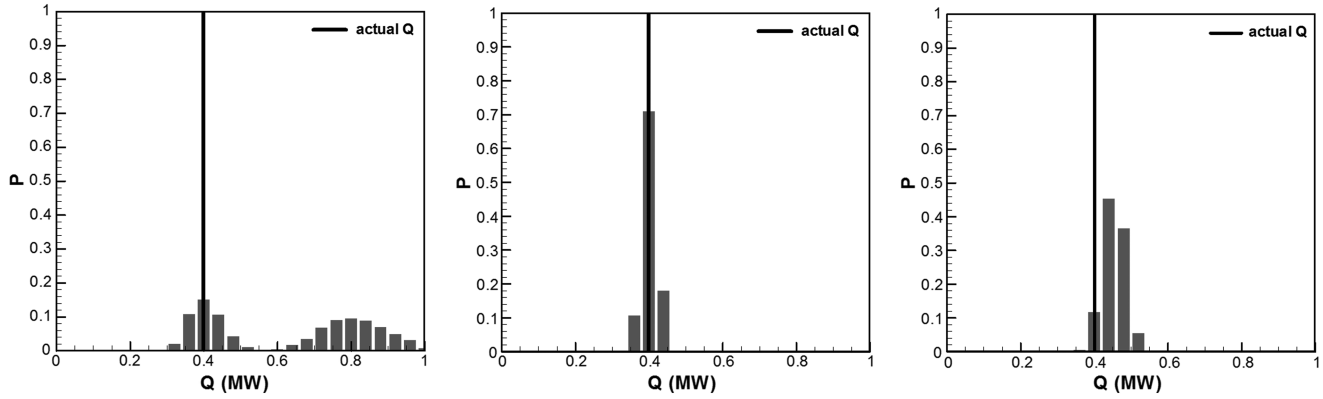

Fig. 8 Histogram (probability) of the fire intensity: a) case 1, b) case 2, and c) case 3.

we can investigate the effects of the sensor network time delay independently from other factors.

Figure 9 shows the fire intensity predicted by the inverse model in all 4 cases. The symbols denote the curves of fire intensity predicted using different amounts of data (data accumulated by 20, 40, 60, and 120 s). The solid lines denote the actual fire intensity curves. From Figs. 9a and 9b, for the case of the variable fire intensity if the sensor network has no time delay, the inverse model can estimate the fire intensity accurately. However, the amount of data required to achieve high accuracy is different (at 60 s in case 1 and at 40 s in case 2) due to different intersensor spacing in the two cases, which is similar to the effect of intersensor spacing for the cases with constant fire intensity discussed in the previous section. Figures 9c and 9d show the estimated fire intensity in case 3 and case 4, in which the time delay of the sensor network is 10 and 20 s, respectively. Comparison of Figs. 9b–9d indicate that increasing time delay has a negative effect on the accuracy of fire intensity estimation. When the delay is 10 s, it is seen that the estimated fire intensity is not consistent with the actual

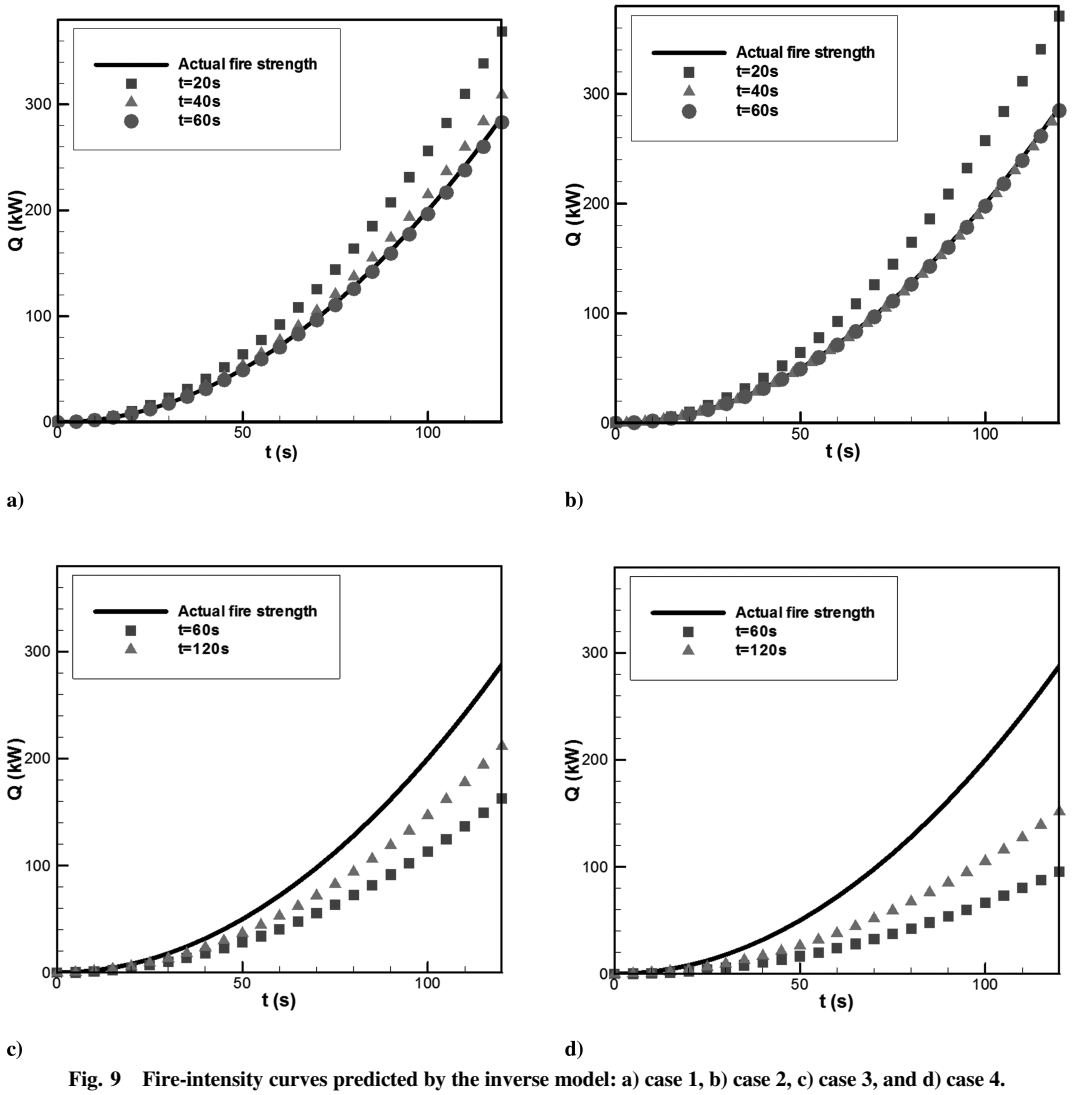

Fig. 9 Fire-intensity curves predicted by the inverse model: a) case 1, b) case 2, c) case 3, and d) case 4.

value for a long time, and even at 120 s, the result is not satisfactory. When the delay increases to 20 s, the discrepancy between the estimated fire intensity with the actual value is more obvious. This can be explained as follows: for case 1, the time delay of the sensor is 10 s, which means that at any given point in time, the readings from the sensor are from 10 s before. So if we do not know the time delay, we will use the sensor readings from 10 s before as if they are the sensor readings at the moment. Thus, the fire strength will be underestimated.

Figure 9 indicates that the time accuracy of a sensor network is an important factor for variable fire intensity inversion. As shown in cases 1 and 2, simulation results indicate that the inversion procedure works well as the amount of accumulated data increases, if the beginning time of the fire is known. In cases 3 and 4, the time delay of the sensor network reduces the accuracy of fire strength estimation. Thus, this effect has to be considered and some extra steps need to be taken in the inversion (e.g., time shifting or translation for the simulation results) in order to obtain accurate estimation of the source parameters.

C. Test 3: Extension to Large Open Spaces

In this section, we extend the fire estimation model to a case with large open space. Figure 10a shows the 17th-floor map of the Jin-Mao building in China, the fifth tallest building in the world. From the figure, it differs from both buildings shown in Fig. 3 of test 1 and in Fig. 7 of test 2, in which there are many separated rooms, and the fire source can be traced back to one of these rooms. The building in this case has large open spaces, and there are few separate zones or rooms. In the center of the 17th floor, there are several equipment rooms. Around the equipment rooms there is a shopping center, like a large cloister surrounding a small atrium. The fire source is located in the top right corner, and the heat release rate is chosen to be a constant value: $Q = 60$ kW.

To deal with the difficulties caused by large open space, in our model, the building is divided into 8 virtual rooms/zones, shown in Fig. 10b. Each virtual room has a height of 2.7 m, a width of 6.0 m and a length of 6.0 m. Every room is connected to its adjacent room through a fully open door. Then in the inverse model, the location of the fire source in a large open space is converted to the localization of the fire source within several virtual rooms, similar to the previous cases.

Temperature sensor readings are obtained by a spatiotemporally well-resolved computational fluid dynamics model (namely, Fire Dynamics Simulator [20]), while the forward numerical simulation is still performed using CFAST, which can make the computation more efficient.

Figure 11 shows the probability distribution (histogram) of the fire location predicted by the inverse model. From the figure, the fire location can be inverted accurately to virtual room 5, where the actual fire is located. The peak posterior probability of fire location is 0.75 in room 5. Here, we did not consider sensor and fire model systematic errors, since the accuracy of the fire location, as mentioned in the previous sections, is not sensitive to systematic errors in the fire model.

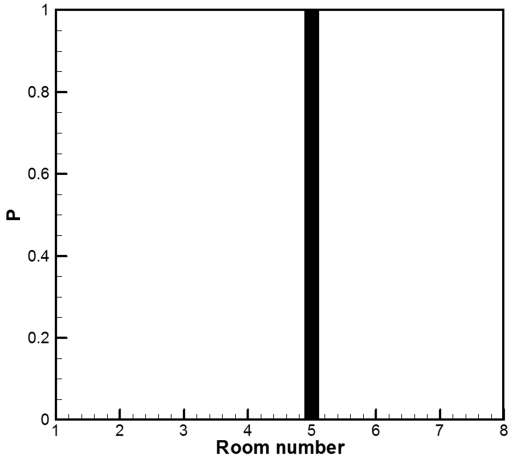

Fig. 11 Histogram (probability) of the fire location.

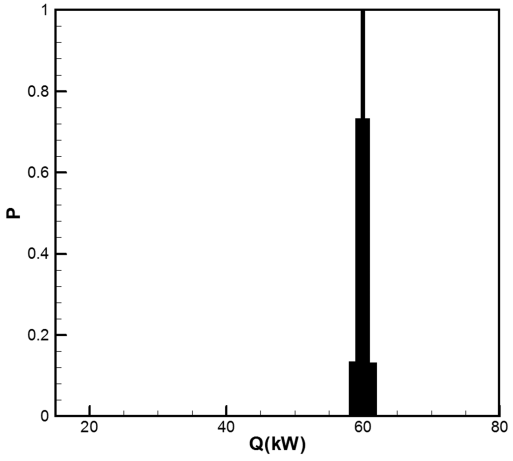

Fig. 12 Histogram (probability) of the fire intensity.

Figure 12 shows the probability distribution (histograms) of the fire intensity predicted by the inverse model, along with the actual intensity 60 kW, denoted as a vertical line. In addition, according to the statistics, the HPD of the estimated fire strength is between 59.13 and 60.92 kW, with a probability of 95%.

IV. Conclusions

The Markov chain Monte Carlo method has been applied to detect the location of a fire source and estimate fire intensity using experimental data and simulations. Our methodology for source inversion

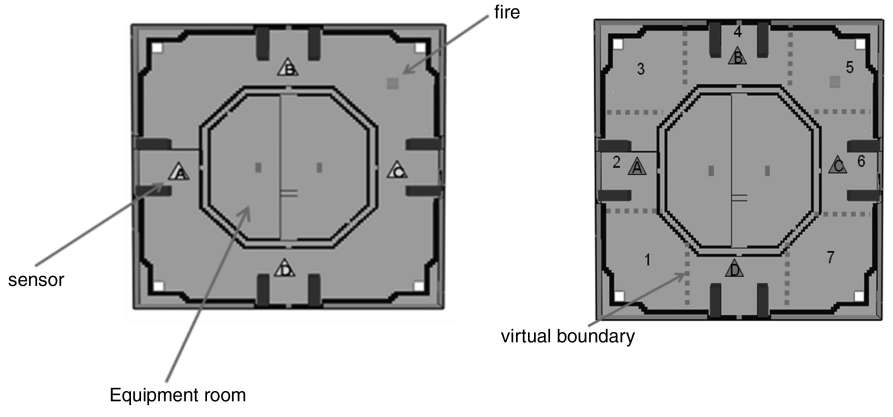

Fig. 10 Configuration of the 17th floor of the Jin-Mao building: a) plan view and b) room partition map.

is based on Bayesian inference. First, a time-dependent temperature database over the entire parameter space was generated using fire simulation models. With the sensor readings and the temperatures simulated by fire models, a likelihood function was assigned, with which the Markov chain Monte Carlo sampling procedure based on Bayesian inference was used to determine parameters such as source location and strength. The probability distributions of the source location and the fire intensity were then calculated by conducting inferences with the Markov chain.

First, a series of multicompartment fire experimental data [19,20] was used to assess the inverse model. The results show that the accuracy of the estimated fire location is not affected by the accuracy of the forward fire model, while the accuracy of fire-intensity estimation by the inverse model is sensitive to the systematic errors or the accuracy of the forward model. If the systematic errors of the forward fire model are added to the inverse model, the estimated fire-source intensity should be improved and agree well with the actual value.

Then another realistic fire scenario in a multiroom building connected by multiple paths was also simulated to investigate the sensitivity and reliability of the model to different types and characteristics of sensor networks. For a constant-intensity fire, we studied the effects of the sensors' time-sampling interval, intersensor spacing, measurement error, working range and time delay. The results show that small time-sampling interval and intersensor spacing will generally result in high estimation performance. However, in some cases, decreasing the intersensor spacing will not significantly improve the accuracy of the estimated intensity, and there exists an optimal combination of time-sampling interval and intersensor spacing, considering the cost. We also discovered that the sensor network with low uncertainty can most accurately estimate the intensity, while the sensor network with high uncertainty may provide insufficient information to distinguish between two possible clusters of the fire intensity. In addition, the sensor network with a lower upper limit can lead to overestimation of the fire intensity. Considering in practice there is often time delay in sensor networks, we also explored the effect of time delay on the accuracy of the inverse model. We found that the discrepancy between the estimated fire intensity and the actual value is large when the time delay is significant. A possible remedy is time shifting or translation for the simulation results. Furthermore, we extended the inverse model to handle cases with fire-intensity variation. The results show that the inverse model can also determine the varying fire intensity accurately with a sufficient amount of time-dependent data, if the beginning time of the fire is known.

Finally, the inverse model was applied to fire-source identification in a large open building structure without separate rooms. In the model, a strategy of virtual zones was used, and the results show that fire-source parameters can be determined with good accuracy.

It is recognized that the scenarios presented in the paper are relatively simple, and the validation and assessment of the inverse model can be improved with future research. More detailed analysis is necessary, for example using more complex building geometries and a wide range of fire sizes to study the effectiveness and efficiency of the model. It is also necessary to study the sensitivity of the model parameters for model improvement. This work is in progress. Furthermore, other elements of sensor networks, such as sensor array geometries, also affect the model performance and will be studied in future research. In addition, we assume the beginning time of the fire is known as prior information. In the future, we are planning to build a system to integrate the current method together with other sensors such as video cameras, which may provide the beginning time of the fire.

Acknowledgments

This work was mainly supported by the Tsinghua–United Technologies Corporation Research Institute for Integrated Building Energy, Safety and Control Systems, and the United Technologies Research Center. The methodology part of the paper was partially supported by National Natural Science Foundation of China (50804027, 70833003). The authors would like to thank Chen Song, Yi Jiang, Yu Guo, and Amit Surana from United Technologies Research Center for their valuable comments and feedback.

References

[1] Richards, R. F., Rabail, R. T., Bakkom, A. W., and Plumb, O. A., "Fire Detection, Location and Heat Release Rate through Inverse Problem Solution. Part II Experiment," *Fire Safety Journal*, Vol. 28, No. 4, 1997, pp. 351–378. doi:10.1016/S0379-7112(97)00006-4

[2] Davis, W. D., and Forney, G. P., "A Sensor-Driven Inverse Zone Fire Model," *Fire Suppression and Detection Research Application Symposium*, Fire Protection Research Foundation, Quincy, MA, 2000, pp. 204–211.

[3] Davis, W. D., Cleary, T., Donnelly, M., and Hellerman, S., "Using Sensor Signals to Analyze Fires," *Fire Suppression and Detection Research Application Symposium*, Fire Protection Research Foundation, Quincy, MA, 2002, pp. 205–224.

[4] Richards, R. F., Munk, B. N., and Plumb, O. A., "Fire Detection, Location and Heat Release Rate through Inverse Problem Solution. Part I Theory," *Fire Safety Journal*, Vol. 28, No. 4, 1997, pp. 323–350. doi:10.1016/S0379-7112(97)00005-2

[5] Chow, F. K., Kosovic, B., and Chan, S., "Source Inversion for Contaminant Plume Dispersion in Urban Environments Using Building-resolving Simulations," *Journal of Applied Meteorology and Climatology*, Vol. 47, No. 6, 2008, pp. 1553–1572. doi:10.1175/2007JAMC1733.1

[6] Liu, X., and Zhai, Z., "Inverse Modeling Methods for Indoor Airborne Pollutant Tracking: Literature Review and Fundamentals," *Indoor air*, Vol. 17, No. 6, 2007, pp. 419–438. doi:10.1111/j.1600-0668.2007.00497.x

[7] Lee, W.-S., and Lee, S.-K., "The Estimation of Fire Location and Heat Release Rate by Using Sequential Inverse Method," *Journal of the Chinese Society of Mechanical Engineers*, Vol. 26, No. 2, 2005, pp. 201–207.

[8] Yang, C.-Y., "Inverse Estimation of Mix-typed Boundary Conditions in Heat Conduction Problems," *Journal of Thermophysics and Heat Transfer*, Vol. 12, No. 4, 1998, pp. 552–561. doi:10.2514/2.6375

[9] Keats, A., Yee, E., and Lien, F. S., "Bayesian Inference for Source Determination with Applications to a Complex Urban Environment," *Atmospheric Environment*, Vol. 41, No. 3, 2007, pp. 465–479. doi:10.1016/j.atmosenv.2006.08.044

[10] Johannesson, G., Hanley, B., and Nitao, J., "Dynamic Bayesian Models via Monte Carlo—An Introduction with Examples," Lawrence Livermore National Lab., TR UCRL-TR-207173, Livermore CA, 2004.

[11] Guo, S., Yang, R., Zhang, H., Weng, W., and Fan, W., "Source Identification for Unsteady Atmospheric Dispersion of Hazardous Materials Using Markov Chain Monte Carlo Method," *International Journal of Heat and Mass Transfer*, Vol. 52, No. 17-18, 2009, pp. 3955–3962. doi:10.1016/j.ijheatmasstransfer.2009.03.028

[12] Liu, X., and Zhai, Z., "Location Identification for Indoor Instantaneous Point Contaminant Source by Probability-based Inverse Computational Fluid Dynamics Modeling," *Indoor air*, Vol. 18, No. 1, 2008, pp. 2–11. doi:10.1111/j.1600-0668.2007.00499.x

[13] Sohn, M. D., Reynolds, P., Singh, N., and Gadgil, A. J., "Rapidly Locating and Characterizing Pollutant Releases in Buildings," *Journal of the Air and Waste Management Association*, Vol. 52, 2002, pp. 1422–1432.

[14] Gelman, A., Bois, F., and Jiang, J., "Physiological Pharmacokinetic Analysis Using Population Modeling and Informative Prior Distribution," *Journal of the American Statistical Association*, Vol. 91, No. 436, 1996, pp. 1400–1412. doi:10.2307/2291566

[15] Andrieu, C., Freitas, N. D., Doucet, A., and Gordan, M. I., "An Introduction to MCMC for Machine Learning," *Machine Learning*, Vol. 50, Nos. 1–2, 2003, pp. 5–43. doi:10.1023/A:1020281327116

[16] Gelman, A., "Inference and Monitoring Convergence," in: Gilks, W. R., Richardson, S., and Spiegelhalter, D. J. (eds.), *Markov Chain Monte Carlo in Practice*, Chapman and Hall, London, 1996, pp. 132–143.

[17] Jones, W. W., and Forney, G. P., "A Programmer's Reference Manual for CFAST, the Unified Model of Fire Growth and Smoke Transport," National Inst. of Standards and Technology, TN 1283, Gaithersburg, MD, 1990.

[18] Guo, S., Yang, R., Zhang, H., Narayanan, S., and Atalla, M., "Development of a Fire Zone Model Considering Mixing Behavior," *Journal of Thermophysics and Heat Transfer*, Vol. 23, No. 2, 2009, pp. 327–338.
doi:10.2514/1.41240

[19] Peacock, R. D., Davis, S., and Lee, B. T., "Experimental Data Set for the Accuracy Assessment of Room Fire Models," National Inst. of Standards and Technology, Rept. NBSIR 88-3752, Gaithersburg, MD, 1988.

[20] McGrattan, K., Hostikka, S., Floyd, J., and Klein, B., "Fire Dynamics Simulator (Version 5) Technical Reference Guide Volume 3: Validation," National Inst. of Standards and Technology, Rept. NISTSP 1018-5, Gaithersburg, MD, 2008.

[21] Dinenno, P. J., Drysdale, D., Beyler, C. L., Walton, W. D., Custer, R. L. D., Hall, J. R., and Watts, J. M., *SFPE Handbook of Fire Protection Engineering*, 3rd ed., National Fire Protection Association, Quincy, MA, 2002.